Specific interfacial area: The missing state variable in two-phase flow equations?

V. Joekar-Niasar[1] and S. M. Hassanizadeh[1]

Received 11 March 2010; revised 17 January 2011; accepted 31 January 2011; published 12 May 2011.

[1] Classical Darcy's equation for multiphase flow assumes that gravity and the gradient in fluid pressure are the only driving forces and resistance to the flow is parameterized by (relative) permeability as a function of saturation. It is conceivable that, in multiphase flow, other driving forces may also exist. This would mean that such nonequilibrium effects are lumped into a permeability coefficient. Indeed, many studies have shown that the relative permeability coefficient generally depends not only on saturation but also on dynamics of the system. Through the application of rational thermodynamics, a theory of two-phase flow had been developed in which interfacial areas were introduced as separate thermodynamic entities and their macroscale effects were explicitly included. This theory includes new driving forces whose significance needs still to be established. To study new terms in the theory, we employ a dynamic pore network model called DYPOSIT. A long pore network (several representative elementary volumes connected in series) is generated, which represents as a one-dimensional porous medium column. This model provides pore scale distribution of local phase pressures, capillary pressure, interfacial area, saturation, and flow rate, which are averaged to obtain the macroscale distributions of these variables. Our analysis shows that there are discrepancies between the simulation results and the classical equations to describe the transient behavior, especially for the nonwetting phase transient permeability. The coefficients in the extended equations are quantified and parameterized. Although under the applied Dirichlet boundary conditions, flow varies significantly, there is a clear trend illustrating dependency of coefficients on saturation, independent of dynamic conditions. Furthermore, using the new coefficients, it is possible to explain either transient or steady state flow regimes, which is a new achievement.

Citation: Joekar-Niasar, V., and S. M. Hassanizadeh (2011), Specific interfacial area: The missing state variable in two-phase flow equations?, *Water Resour. Res., 47*, W05513, doi:10.1029/2010WR009291.

1. Introduction

1.1. Theories of Two-Phase Flow Including Interfacial Area

[2] In the literature, there are extensive experimental, theoretical, and computational investigations of different properties of multiphase systems, which are directly related to the topology and property of fluid-fluid interfaces and capillary forces acting on them. Of these studies, we can refer to calculation of effective viscosity in viscous fingering regime [*Koval*, 1963; *Sorbie et al.*, 1995], averaging the phase pressures [*Zhang et al.*, 2007; *Nordbotten et al.*, 2007; *Yang et al.*, 2009; *Korteland et al.*, 2009], scaling of the fingering with dynamic properties of a system [*Tallakstad et al.*, 2009], crossover behavior from viscous fingering to compact flow or from capillary fingering to viscous fingering [e.g., *Wilkinson*, 1986; *Fernández et al.*, 1991; *Ferer et al.*, 1993], nonequilibrium relative permeability curves [e.g., *Goode and Ramakrishnan*, 1993; *Tsakiroglou et al.*, 2003; *Theodoropoulou et al.*, 2005], relaxation time in fluid distribution [e.g., *Buyevich*, 1995], etc. Many of these issues cannot be explained by classical Darcy's law for multiphase flow.

[3] In the so-called extended Darcy's law for multiphase flow, it is assumed that the only driving forces for flow of each fluid are the gravity and the gradient in fluid pressure. The resisting force, which balances the driving force, is assumed to be linearly proportional to the relative fluid velocity with respect to the solid. This results in a linear relationship between the flow velocity and driving forces. While these assumptions are reasonable for single-phase flow, one may expect many other factors to affect the balance of forces in the case of multiphase flow. Among these are the interfacial forces that influence the movement of phases and the distribution of interfaces in a porous medium. In fact, through the application of rational thermodynamics, *Hassanizadeh and Gray* [1990, 1993a] developed a theory of two-phase flow in which interfacial areas were introduced as separate thermodynamic entities, possessing mass, momentum, and energy. They derived the momentum balance equations not only for phases but also for the interfaces, and macroscale effects of interfacial forces were

[1]Environmental Hydrogeology Group, Department of Earth Sciences, Utrecht University, Utrecht, Netherlands.

0043-1397/11/2010WR009291

explicitly included. They found that the driving forces for the flow of a phase were the gradients of Gibbs free energy of the phase plus gravity. They showed that for the case of single-phase flow, the gradient of Gibbs free energy reduces to the gradient of pressure. But, for the case of two-phase flow, because the Gibbs free energy of a phase is a function of saturation and specific interfacial area, as well as mass density, its gradient will lead to terms in addition to the pressure gradient. They derived the following extended form of Darcy's law in which the gradients of pressure, saturation, and specific interfacial area appeared as driving forces:

$$\mathbf{v}^{\alpha} = -\frac{\mathsf{K}^{\alpha}}{\mu^{\alpha}} \cdot \left(\nabla P^{\alpha} - \rho^{\alpha}\mathbf{g} - \Psi^{\alpha a}\nabla a^{nw} - \Psi^{\alpha S}\nabla S^{w}\right), \quad \alpha = w, n, \tag{1}$$

where $\mathbf{v}^{\alpha}$ denotes the relative velocity of fluid phase α with respect to the solid. In the rest of this work, without loss of generality, we assume that the solid phase is rigid. K^{α} is α phase permeability tensor, $\Psi^{\alpha a}$ and $\Psi^{\alpha S}$ represent material properties, $\mathbf{g}$ is the gravity vector, a^{nw} is the specific area of fluid-fluid interfaces (amount of interfacial area per unit volume of the porous medium), and P^{α}, ρ^{α}, S^{α}, and μ^{α} are pressure, mass density, saturation, and viscosity of the α phase, respectively. Superscripts w and n designate wetting and nonwetting phases, respectively. Note that K^{α} is the product of relative permeability coefficient and the absolute permeability tensor. Thus, in the new formulation of two-phase flow, it is considered to be a function of the average saturation. In the classical Darcy's law, without the new added terms in equation (1), it has been illustrated experimentally and computationally that K^{α} is not only a function of saturation but also the dynamic conditions of the system. Those pore scale studies, which have investigated this issue experimentally, have been reviewed by *Joekar-Niasar and Hassanizadeh* [2011].

[4] *Hassanizadeh and Gray* [1990, 1993a] also showed that the average motion of fluid-fluid interfaces is also due to a gradient in their Gibbs free energy plus gravity. Again, as the Gibbs free energy of interfaces is a function of saturation and specific interfacial area, the following equation for the average velocity of fluid-fluid interfaces was obtained:

$$\mathbf{w}^{nw} = -\mathsf{K}^{nw} \cdot \left[\nabla(a^{nw}\sigma^{nw}) + \Psi^{nw}\nabla S^{w}\right]. \tag{2}$$

[5] In equation (2), $\mathbf{w}^{nw}$ denotes the relative macroscopic velocity of fluid-fluid interfaces with respect to the solid, K^{nw} is the permeability tensor for *nw* interfaces, Ψ^{nw} represents a material property, and σ^{nw} is the macroscale interfacial tension. Note that the effect of gravitational forces on the movement of interfaces is neglected. Thus, the gravity term $\mathbf{g}$ has been neglected in equation (2). These equations may be seen as the truly extended forms of Darcy's law, not only for a fluid phase but also for an interface. They must be supplemented with the following equations of balance of volume for phase saturations and specific interfacial area (assuming incompressible phases and constant mass density for interfaces):

$$\varphi\frac{\partial S^{\alpha}}{\partial t} + \nabla \cdot \mathbf{v}^{\alpha} = 0, \quad \alpha = w, n, \tag{3}$$

$$\frac{\partial a^{nw}}{\partial t} + \nabla \cdot (a^{nw}\mathbf{w}^{nw}) = E^{nw}, \tag{4}$$

where φ is the porosity, $\mathbf{v}^{\alpha}$ and $\mathbf{w}^{nw}$ denote the average velocities of α phase and *nw* interfaces, respectively, and E^{nw} is the net rate of production of *nw* interfaces. It is proposed that E^{nw} should depend on saturation and its time rate of change [*Pop et al.*, 2009; *Niessner and Hassanizadeh*, 2008]. *Joekar-Niasar et al.* [2010a] studied dependence of E^{nw} on dynamic parameters (viscosity ratio and different global pressure difference) using a dynamic pore network model. But, the size of the network was almost one representative elementary volume (REV), and they assumed that the advective flux of specific interfacial area was negligible. Here, the full set of equations are analyzed in a network of several REVs in series.

[6] Another central equation in the theories of two-phase flow is the so-called capillary pressure–saturation relationship, which is commonly written as

$$P^{n} - P^{w} = P^{c}(S^{w}). \tag{5}$$

[7] In fact, there are two major assumptions in equation (5): capillary pressure is a function of wetting phase saturation only, and fluids pressure difference is equal to capillary pressure (at all times and under all conditions). Regarding the first assumption, it is known that the capillary pressure–saturation relationship is not unique but function of the history of fluids movements, even though it is obtained under equilibrium conditions. This is probably because the P^c-S^w relationship depends not only on the volume fraction of phases but also on their microscale distribution [*Entov*, 1980]. In fact, one would expect the capillary pressure to depend also on the interfacial curvature (similar to Laplace law at pore scale) and/or specific interfacial area. *Hassanizadeh and Gray* [1993b] have suggested that the nonuniqueness in the capillary pressure–saturation relationship is indeed due to the absence of specific interfacial area in the capillarity theory, and they proposed the following equation for the macroscopic capillary pressure:

$$P^{c} = P^{c}(S^{w}, a^{nw}). \tag{6}$$

[8] A number of computational and experimental works have shown that under a wide range of drainage and imbibition histories, P^c-S^w-a^{nw}surfaces more or less coincide [e.g., *Reeves and Celia*, 1996; *Cheng et al.*, 2004; *Joekar-Niasar et al.*, 2008, 2009, 2010b; *Porter et al.*, 2009]. This means that the inclusion of a^{nw} leads to the removal or significant reduction of hysteresis in the capillary pressure–saturation relationship. In other words, a unique P^c-S^w-a^{nw}surface may exist for all the imbibition and drainage process.

[9] Regarding the second assumption underlying equation (5), it is now an established fact that $P^n - P^w$ is equal to the capillary pressure but only under equilibrium conditions (see *Hassanizadeh et al.* [2002] for an extended review of experimental evidences). For nonequilibrium situations, the following equation for the difference in fluid pressures has been suggested [*Stauffer*, 1978; *Entov*, 1980; *Kalaydjian and Marle*, 1987; *Hassanizadeh and Gray*, 1990]:

$$P^{n} - P^{w} = P^{c} - \tau\frac{\partial S^{w}}{\partial t}, \tag{7}$$

where τ, the nonequilibrium capillarity coefficient, is a material property that may still be a function of saturation and specific interfacial area.

[10] V. Joekar-Niasar and coworkers analyzed the behavior of τ as a function of saturation for different viscosity ratios under drainage [*Joekar-Niasar et al.*, 2010a] and imbibition [*Joekar-Niasar and Hassanizadeh*, 2010] conditions. They found that there is a significant nonequilibrium effect especially for favorable viscosity ratios. Recently, *Niessner and Hassanizadeh* [2008] have set up a numerical model based on equations (1)–(6). They have shown that the extended model can properly capture physical processes such as capillary hysteresis. They have also shown that the introduction of interfacial area provides a physically based model of kinetic mass and heat transfer [*Niessner and Hassanizadeh*, 2009a, 2009b].

[11] The physical behavior of various coefficients in the proposed set of equations is not fully analyzed. In particular, the behavior of equations (1), (2), and (4) has not been investigated in any laboratory works because of the technical limitations. Even if experiments are possible, it would be valuable to have an idea of the potential significance of various terms appearing in these equations and to obtain information on the order of magnitude of corresponding coefficients. This can be done with the aid of pore scale simulations. We have chosen the pore network modeling because of its rather low computational costs, which allows us to simulate larger domains compared to the other pore scale simulators. Pore network models are classified under quasi-static and dynamic ones, which are both employed in this study. Details of the quasi-static pore network models, as the most common pore scale simulator, are given by *Joekar-Niasar et al.* [2008].

1.2. Dynamic Pore Network Modeling

[12] Dynamic pore network models can simulate the distribution of fluids and their local pressure values under static, steady state, and transient conditions in an idealized porous medium. However, they have been mostly used for analysis of the transient behavior. Under static conditions, there is no pressure gradient over the network and there is no flow at the pore scale and Darcy scale (there is no change in saturation and all interfaces are at rest). Under the steady state conditions, the saturation values do not change with time and the interfaces are at rest too, but there is a pressure gradient over the domain, and thus the fluids flow at the pore scale as well as the Darcy scale. Under transient conditions, the fluid-fluid interfaces move with time and the saturation changes at both local and Darcy scales. The first dynamic pore network model reported in the literature was developed by *Koplik and Lasseter* [1985], who simulated two-phase imbibition process in a two-dimensional unstructured pore network model with circular cross sections. Later, several dynamic pore network models were developed for various applications, such as simulating two-phase drainage [e.g., see *Aker et al.*, 1998; *Al-Gharbi and Blunt*, 2005; *Dahle and Celia*, 1999; *Gielen et al.*, 2005; *Nordhaug et al.*, 2003], imbibition [e.g., see *Koplik and Lasseter*, 1985; *Hughes and Blunt*, 2000; *Thompson*, 2002], evaporation [e.g., *Prat* 2002], and three-phase flow [e.g., see *Pereira et al.*, 1996]. Of notable significance are the models developed by Payatakes and coworkers [see, e.g., *Constantinides and Payatakes*, 1996; *Dias and Payatakes*, 1986a, 1986b], which could simulate the ganglia displacement.

[13] Recently, *Joekar-Niasar et al.* [2010a] and *Joekar-Niasar and Hassanizadeh* [2010] developed a dynamic two-phase model for simulating both drainage and imbibition, called DYPOSIT: DYnamic Pore network SImulator for Two-phase flow. This model has a number geometrical and numerical advantages compared to the previous ones, which are explained in detail by *Joekar-Niasar et al.* [2010a]. The model solves two pore scale pressure fields, one for each phase, in a network with angular cross sections. The pressure fields are related to each other through the local capillary pressure, which is a function of local interface curvature and subsequently local pore body saturation. The model remains stable for both drainage and imbibition within a wide range of viscosity ratios and capillary numbers.

1.3. Objectives

[14] The purpose of this work is to provide insight into the behavior and potential significance of various terms ($\Psi^{\alpha a}$ and $\Psi^{\alpha S}$, $\alpha = w, n$ in equation (1), Ψ^{nw} and K^{nw} in equation (2), and E^{nw} in equation (4)) in the extended theories of two-phase flow in porous media, presented above. We perform the transient drainage simulations in a long pore network, representing a one-dimensional column. After finishing the pore scale simulations, postprocessing analysis is performed to obtain the Darcy-scale entities introduced in the theory. A moving REV averaging procedure is formulated that results in the macroscale fields of fluids pressures, velocities, saturations, and specific interfacial area. Finally, with extensive analysis of these data, the functional dependencies and magnitudes of coefficients $\Psi^{\alpha a}$, $\Psi^{\alpha S}$, Ψ^{nw}, K^{nw}, and E^{nw} are obtained.

2. Model Description

[15] In this study, we have used a dynamic pore network simulator for two-phase flow, DYPOSIT, developed by *Joekar-Niasar et al.* [2010a] and *Joekar-Niasar and Hassanizadeh* [2010]. Here, a summary of main features, governing equations for pore scale simulations, and algorithms are provided. Please note that all entities introduced in this section are local (pore scale) entities. To employ results of simulations for the analysis of Darcy-scale equation, the pore scale entities should be averaged. Details of the averaging procedure are introduced in section 3.4.

2.1. Structure and Geometry

[16] The network is based on a regular three-dimensional lattice with fixed coordination number of six. Table 1 shows fluid and network properties used in the simulations. Length of the network in the flow direction is equal to 210 pore bodies. Over the network cross section normal to the flow direction, there are 30 $\times$ 30 pore bodies. Given the definition of the viscosity ratio as $(M = \mu^{\text{invading}}/\mu^{\text{receding}})$, it can be smaller than one (in oil recovery) or larger than one (in fuel cells, paper pulp industry). We select $M = 1$ as it is the most neutral case; under Dirichlet boundary conditions with invasion of a fluid, the interface pattern can change from a stable front to a capillary fingering one.

Table 1. Fluid and Network Properties Used in the Simulations and Analyses

Parameter	Symbol	Value	Unit
Contact angle	θ	0.0	degree
Interfacial tension	σ^{nw}	0.0725	kg s^{-2}
Wetting fluid viscosity	μ^w	0.001	kg m^{-1} s^{-1}
Nonwetting fluid viscosity	μ^n	0.001	kg m^{-1} s^{-1}
Total number of pore bodies in flow direction	n_z	210	-
Total number of pore bodies in lateral directions	n_x, n_y	30	-
Network size	-	$7.28 \times 1.08 \times 1.08$	mm^3
Permeability (calculated)	K	6.56×10^{-12}	m^2
Entry capillary pressure (calculated)	P_d^c	14	kPa

[17] Pore bodies and pore throats are represented by "cubes" and "parallelepipeds," respectively (Figure 1). The size distribution of pore bodies is specified by a truncated lognormal distribution. No spatial correlation has been considered in the network, as the effect of correlation length on the simulation results is out of the focus of this study. Statistical properties of radii of pore body inscribed spheres, pore throat inscribed circles, and aspect ratio distributions are shown in Table 2. Aspect ratio is defined as the ratio of the radius of a pore body to that of a pore throat. Corresponding to Table 2, Figures 2a and 2b show the pore body and pore throat size distributions as well as aspect ratio distribution.

2.2. Assumptions

[18] The following assumptions are imposed in the computational algorithm and network development.

[19] 1. The volume of pore throats is negligible compared to the volume of pore bodies. Thus, the time required for filling a single pore throat is negligible compared to that of a pore body. This assumption is in agreement with the experiments which measured the velocity of Haines jump

Table 2. Statistical Properties of the Radii of Inscribed Spheres in Pore Bodies (R_i) and Inscribed Circles in Pore Throats r_{ij}

Specifications	R_i (mm)	r_{ij} (mm)
Min	0.008	0.005
Max	0.018	0.013
Mean	0.012	0.008
SD	0.003	0.0017

[*Lu et al.*, 1994]. Also, the volume and interfacial area of pore throats are not included in the computation of network saturation and specific interfacial area.

[20] 2. Hydraulic resistance to flow in pore bodies is assumed to be negligible compared to that of pore throats.

[21] 3. Fluids are assumed to be immiscible and incompressible, and the solid matrix is assumed to be rigid.

[22] 4. Flow in the pore throats is assumed to have a low Reynolds number such that transient effects can be neglected at pore scale. This allows us to use *Washburn*-type [*Washburn*, 1921] equation for fluid fluxes through pores.

[23] 5. No gravity effect has been considered in the simulations. Flow occurs owing to the pressure difference across the boundaries. Adding gravity does not constitute any major complication in the code, but it will not affect results and conclusions.

2.3. Two-Phase Flow Formulations for the Network Model

2.3.1. General Equations for the Two-Phase Flow

[24] The local capillary pressure for a pore body i, p_i^c, is defined as

$$p_i^c = p_i^n - p_i^w = f(\kappa_i) = f(s_i^w), \tag{8}$$

where p_i^n and p_i^w are the local fluid pressures, κ_i is the curvature of an interface within the pore body i, and s_i^w is defined as the volume of the wetting fluid in a pore body divided by the volume of the pore body. Since the fluid

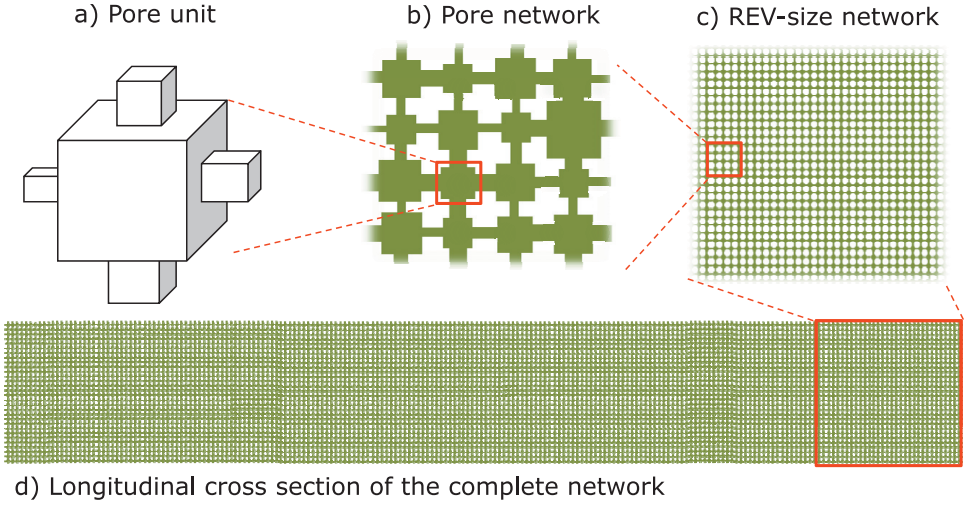

Figure 1. Illustration of the network and its elements. (a) A pore unit. (b) A part of the REV-size network. (c and d) The complete network in 2-D.

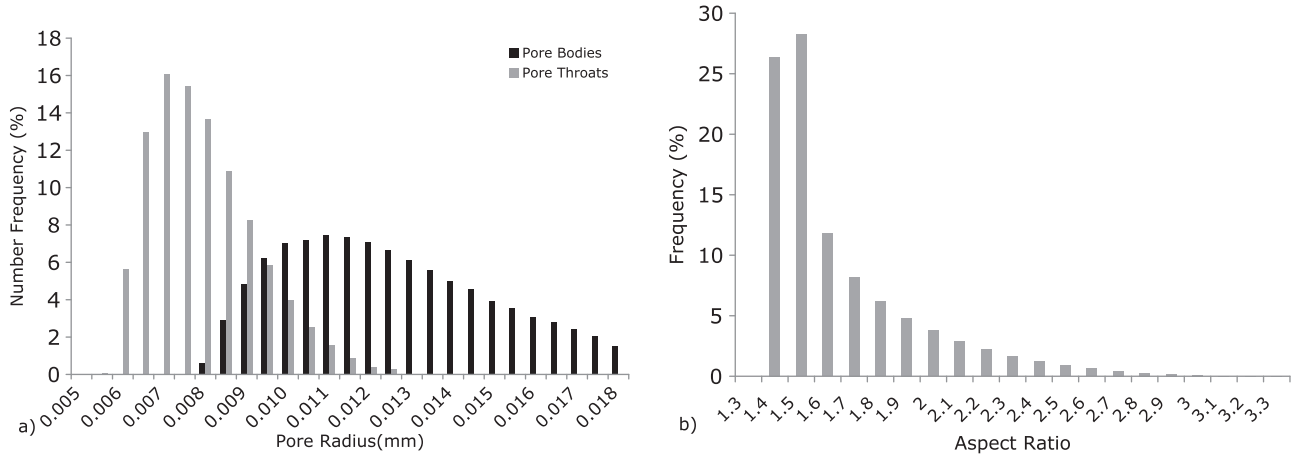

Figure 2. Network geometry properties. (a) Pore body and pore throat size distributions. (b) Aspect ratio distribution.

configuration at pore scale is constrained by solid boundaries, there is a unique algebraic relationship between the local curvature and local wetting phase saturation. Note that compared to equation (7), no relaxation time is assumed to exist in a change of the curvature due to the change of fluid pressures. So, the term $\tau \partial S^w / \partial t$ in equation (7) is due to the spatial rearrangement of fluids over the whole network in order to reach the equilibrium. It means that under transient conditions, although at the pore scale κ_i varies spontaneously with change of local phase pressures with time, at the Darcy scale there will be a nonequilibrium effect in reaching to Darcy-scale equilibrium saturation.

[25] A flux Q_{ij}^{α} is assigned to a pore throat ij for each phase separately. A separate volume balance for each phase in a pore body is employed:

$$V_i \frac{\Delta s_i^{\alpha}}{\Delta t} = -\sum_{j \in N_i} Q_{ij}^{\alpha}, \ \alpha = w, n, \tag{9}$$

where N_i is the set of all pore throats connected to pore body i, V_i is the volume of the pore body, and s_i^{α} is the saturation of phase α in the pore body. Washburn's formula [*Washburn*, 1921] was originally developed for circular cross sections. Analogous to that, the volumetric flux of phase α in an angular cross-sectional pore throat ij is given by

$$Q_{ij}^{\alpha} = -\mathsf{K}_{ij}^{\alpha}(p_j^{\alpha} - p_i^{\alpha}), \quad \alpha = w, n, \tag{10}$$

where K_{ij}^{α} is an algebraic function of the geometry and fluid occupancy of the pore throat given by *Joekar-Niasar and Hassanizadeh* [2010].

[26] Most dynamic pore network models assign one single fluid pressure to a pore body and single effective conductivity to a pore throat [see, e.g., *Al-Gharbi and Blunt*, 2005; *Mogensen and Stenby*, 1998]. Here, we assign different pressures and conductivities to each phase. This has major advantages. For example, it allows us to include mechanisms related to the local capillary pressure (such as snap-off, countercurrent flow, mobilization of discontinuous phases). Equations (8), (9), and (10) form a determinate set to be solved for s_i^w, p_i^w, and p_i^n. The pressure fields and saturation are calculated in sequence. Details of formulations employed for pressure and saturation as well as time stepping are explained by *Joekar-Niasar et al.* [2010a]. To improve numerical stability of the model for different dynamic conditions, a semi-implicit saturation update has been used. Thus, two linear systems of equations were solved for pressure and saturation by diagonally scaled biconjugate gradient method using the SLATEC mathematical library (http://www.netlib.org/slatec/guide).

2.3.2. Local Rules

2.3.2.1. Capillary Pressure–Saturation Relationships for Pore Bodies and Pore Throats

[27] Since pore bodies in our model are cubic, the wetting phase is always present in the corners and along edges. The saturation of the pore body depends on the prevailing capillary pressure. For a given capillary pressure, curvature of the interface in the vertices and edges of the cube can be calculated, and consequently, the corresponding saturation can be estimated. Details of derivation of the (local) p_i^c-s_i^w relationship for a cubic pore body are given by *Joekar-Niasar et al.* [2010a]. The resulting equation for p_i^c in terms of the radius R_i of the inscribed sphere of the pore body i and the local wetting phase saturation is

$$p_i^c(s_i^w) = \frac{2\sigma^{nw}}{R_i[1 - \exp(-6.83 s_i^w)]}. \tag{11}$$

[28] A capillary pressure should be also assigned to a pore throat once it is invaded and both phases are present. We assume that the capillary pressure in a pore throat is equal to the capillary pressure of the upstream pore body.

[29] Obviously, it is impossible to completely displace the wetting phase from the corners of a pore body. We assume that each pore body has a minimum saturation $s_{i,\min}^w$, which depends on the imposed global pressure difference (P_{global}^c defined in section 3.1) as well as the blockage of the invading fluid. The capillary blockage of invading fluid $\left(P_{e_{\text{block}}}^c\right)$ is also a global variable, defined to be the minimum entry capillary pressure of all pore throats that are in the vicinity of the nonwetting phase but not invaded

by it yet. Thus, using the p_i^c-s_i^w relationship given by equation (11), the local minimum wetting phase saturation in a pore body may be determined as follows:

$$s_{i,\min}^{w} = -\frac{1}{6.83}\ln\left[1 - \frac{1}{R_i}\frac{2\sigma^{nw}}{\min\left(P^c_{\text{global}}, P^c_{e_{\text{block}}}\right)}\right]. \quad (12)$$

2.3.2.2. A_i^{nw}-s_i^w Relationship for a Pore Body

[30] In our calculations, we consider only the interfacial area existing in pore bodies. There are two different types of capillary interfaces in a pore body, interfaces in corners and edges and interfaces covering the entrance of pore throats that have not yet been invaded. These two types are referred to as "corner interfaces" (arc menisci) and "main terminal menisci," respectively [*Mason and Morrow*, 1987]. Detailed information for calculation of interfacial area is given by *Joekar-Niasar et al.* [2010a].

[31] For corner interfaces ($A_{c_i}^{nw}$), given a pore body with inscribed radius R_i and filled with both phases, the nonwetting phase volume can be smaller or larger than the inscribed sphere volume. If the nonwetting phase volume is smaller than or equal to the volume of inscribed sphere (corresponding to $s_i^w \geq 0.48$), we assume that it occupies a sphere, the radius of which is $R_{i,eq} = R_i\left[6/\pi(1-s_i^w)\right]^{1/3}$. The corresponding interfacial area will be $4\pi R_{i,eq}^2$. If the nonwetting phase volume is larger than the volume inscribed sphere (corresponding to $s_i^w < 0.48$), the total interfacial area in corners of a pore body will be equal to $4\pi R_{i,eq}^2 + 6\pi R_{i,eq}(R_i - R_{i,eq})$, where $R_{i,eq}$ is defined in equation (13). The results are summarized as follows:

$$R_{i,eq} = \begin{cases} R_i[\frac{6}{\pi}(1-s_i^w)]^{1/3} & s_i^w \geq 0.48 \\ R_i[1-\exp(-6.83 s_i^w)] & s_i^w < 0.48 \end{cases} \quad (13)$$

$$A_{c_i}^{nw} = \begin{cases} 4\pi R_{i,eq}^2 & s_i^w \geq 0.48 \\ 4\pi R_{i,eq}^2 + 6\pi R_{i,eq}(R_i - R_{i,eq}) & s_i^w < 0.48 \end{cases} \quad (14)$$

[32] For the main terminal menisci ($A_{m_i}^{nw}$), consider a pore body i, partially occupied by the nonwetting phase, and a pore throat ij, which has not been yet invaded. Opening of the pore throat ij is thus covered by a "main terminal meniscus." The geometry of the main terminal meniscus is simply assumed to be a part of a sphere with a radius of curvature R_{dm} equal to $2\sigma^{nw}/P_i^c$. Thus, the area of the main terminal meniscus will be equal to $A_{m_i}^{nw} = 8\pi\left(\sigma^{nw}/P_i^c\right)^2 \times \left(1 - \sqrt{1 - \left(r_{ij}P_i^c/2\sigma^{nw}\right)^2}\right)$, i is the upstream pore body of pore throat ij. Thus, the total interfacial area (A_i^{nw}) in a pore body is equal to $A_i^{nw} = A_{c_i}^{nw} + A_{m_i}^{nw}$.

[33] In addition to the local capillary pressure–saturation and the local interfacial area-saturation curves, relations for the entry capillary pressure of pore throats, phase conductivities of pore throats, and snap-off condition in pore throats should be defined. Details of these relations are given by *Joekar-Niasar et al.* [2010a].

3. Simulations and Analysis

3.1. Network Size and Boundary Conditions

[34] To analyze Darcy-scale equations using pore network models, size of the pore network should be equal to at least one REV. It should be noted that REV size will increase with the increase of (1) the variance of pore size distribution, (2) the correlation length in the spatial pore size distribution, and (3) the heterogeneity in network topology. In the network modeling concept, various REV sizes have been reported in the literature. For example, *Nordhaug et al.* [2003] selected a lattice network with size of 10 pore bodies as the REV for studying the macroscopic interface velocity. *Al-Gharbi and Blunt* [2005] analyzed dependencies of fractional flow curves on dynamic conditions in a 9 × 9 two-dimensional network. For reactive transport studies, *Li et al.* [2007] selected a network with a total of 6000 pores as the REV. The REV selected by *Gielen et al.* [2005] was equal to a lattice network with 10 pore bodies in each direction. They quantified the nonequilibrium capillarity coefficient during drainage.

[35] In this study, we have determined the size of REV on the basis of P^c-S^w and k_r^α- S^w curves, which are the main characteristic curves for a porous medium. The size of REV was determined by performing equilibrium drainage simulations in networks with different sizes but the same statistical parameters. The capillary pressure–saturation (P^c-S^w) and the relative permeability-saturation (k_r^α-S^w) curves, resulting from the networks with different sizes, were compared to each other. Our simulation results (not presented) showed that these characteristic curves were identical for networks larger than 30 × 30 × 30 pore bodies. Thus, for given statistical parameters, the REV is a lattice network with 30 pore bodies in each direction. This size of REV is quite large compared to the typical REV sizes reported in the literature. So, for our simulations, we constructed a pore network model with the cross-sectional size of 30 × 30 pore bodies. To be able to calculate the gradients of pressures, saturation, and interfacial area from pore network simulations, a long pore network model was required. Thus, the length of network was chosen to be equal to 210 pore bodies along the flow direction. The simulation of drainage process in this network took more than 3 weeks using one processor of an AMD Opteron 2218 computer with 6GB RAM.

[36] For our simulations, we assumed that the network was connected to a nonwetting phase reservoir on one side and a wetting phase reservoir on the other side. Phase pressures were specified at these boundaries. Side boundary conditions were assumed to be periodic.

[37] The pressure of the nonwetting phase reservoir was denoted by P^n_{top}, and the pressure of the wetting phase reservoir was set to zero. The difference between the two boundary pressures during drainage is referred to as "global pressure difference" P^c_{global}. P^c_{global} in our simulation was set to 30 kPa. Once the nonwetting phase reached a pore throat at the wetting phase boundary, it was assumed that the gradient of capillary pressure within the invaded pore throat was equal to zero ($\partial p_{ij}^c/\partial l_{ij} = 0$). This was done to prevent a sudden relaxation of interfaces after breakthrough of the nonwetting fluid.

3.2. Drainage Simulations

[38] The network was assumed to be initially fully saturated with the wetting phase. Simulation started with raising the pressure of the nonwetting phase reservoir to P^n_{top} and establishing a global pressure difference, P^c_{global}, across the network. When the imposed pressure difference was larger than the entry pressure of the largest pore throat at the nonwetting phase reservoir boundary, drainage would start. In quasi-static simulations, the nonwetting phase reservoir pressure was increased in incremental steps so that the network would be invaded in steps. At the end of each step, when there was no flow (static conditions), the overall saturation and the specific interfacial area were determined. Then the global pressure difference was increased again. Each global pressure difference corresponds to a saturation value. The capillary pressure–saturation data points formed the quasi-static P^c-S^w curve. In transient simulations, the imposed P^c_{global} was chosen to be so large that the whole network could be flooded in one transient step. The simulations were continued until the change of average saturation in the whole network was not significant.

3.3. Steady State Phase Permeability Curves

[39] Relative permeability for each phase is commonly determined from the steady state flow experiments as a function of average saturation. A steady state flow experiment at a given average saturation (or a given capillary pressure) was simulated as follows. As described above, in quasi-static simulations, we obtained an equilibrium configuration of fluids in the network at a given P^c_{global}. That equilibrium configuration was frozen, and a small pressure gradient for each phase was imposed across the selected section of the network, where both phases formed a continuous path. The pressure gradient was chosen such that the imposed P^c_{global} was kept unchanged at the boundaries. Also, it was assumed to be so small that fluid configurations were not affected. Therefore, equations (8)–(10) would apply with the left-hand side of equation (9) being zero. The solution of resulting equations provided steady state pressure fields for the two phases. Then total flow through the network for each phase was calculated. Then, following the classical Darcy's law, the phase permeability K^α was calculated as $-\mu^\alpha \mathbf{v}^\alpha / (\partial p^\alpha / \partial x)$. One should note that since the pore throats have square cross sections, wetting fluid is always connected to the reservoir, but its conductance decreases with increase of global capillary pressure P^c_{global}.

3.4. Averaging Procedure and Averaging Operators

[40] Our simulations resulted in the fields of local variables, such as pressures, saturations, and fluxes, at consecutive time steps. These were then averaged over an averaging domain moving along the network. That is, at any given time, t, the averaging domain was moved along the network pore layer by pore layer; thus, determining average variables as a function of distance x (position of the center of the averaging domain; see Figure 3). This allowed us to obtain gradients of average variables as well as their time derivatives. The averaging domain size was chosen to be 30 × 30 × 30 pores, which we had determined to be the REV size. Thus, for our network with the length of 210 pore bodies, this procedure resulted in 180 values for each average variable, at any given time. Average values were determined

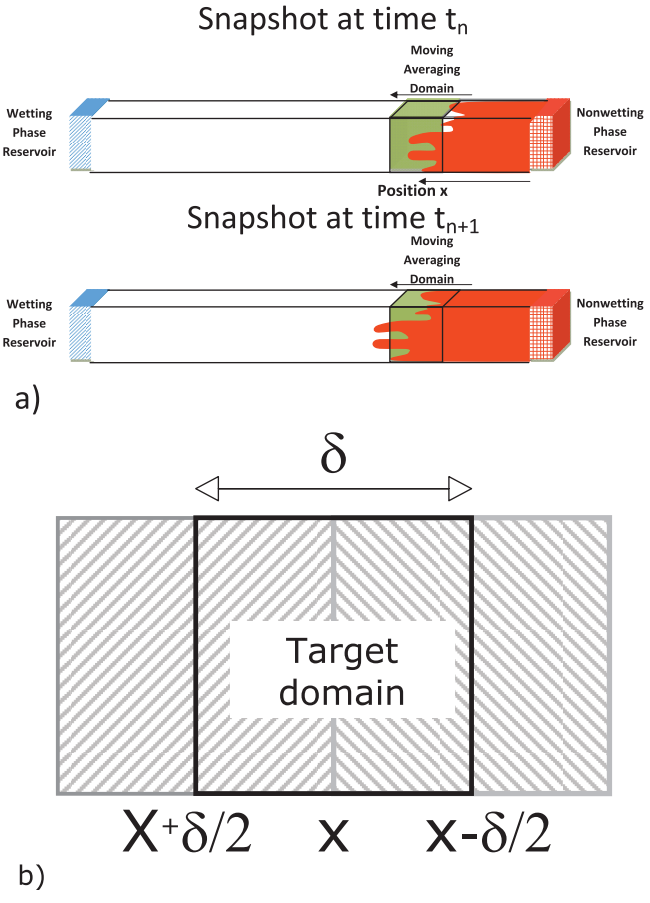

Figure 3. (a) Schematic presentation of averaging domain moving along the flow direction. (b) For calculating the gradient of average variables, average values at two neighboring domains centered at $x - \delta/2$ and $x + \delta/2$ are used.

for saturation, specific interfacial area, pressure, fluid velocities, and interface velocity, following formulas presented below.

[41] Average saturation was simply defined as the ratio of total volume of the wetting phase within the averaging domain to the total pore volume:

$$S^w = \frac{\sum_{j=1}^{n^{pb}} s_j^w V_j}{\sum_{j=1}^{n^{pb}} V_j}, \tag{15}$$

where V_j is the volume of pore body j and n^{pb} is the total number of pore bodies of the averaging domain centered at x. The gradient of saturation for domain was calculated from the average saturations of domains centered at $x - \delta/2$ and $x + \delta/2$, as shown in Figure 3b:

$$\frac{\partial S^w}{\partial \mathrm{x}} = \frac{S^w_{x+\delta/2} - S^w_{x-\delta/2}}{\delta}, \tag{16}$$

where δ is the length of the averaging domain.

[42] The averaging of pressure is less straightforward. Commonly, average pressure is obtained using an intrinsic phase average operator [see, e.g., *Whitaker*, 1977]. However, recently it has been shown that the intrinsic phase average pressure introduces numerical artifacts when both

pressure and saturation are spatially variable [see *Nordbotten et al.*, 2007, 2008; *Korteland et al.*, 2009]. Instead, a centroid-corrected averaging operator has been suggested by *Nordbotten et al.* [2008] to alleviate problems associated with intrinsic phase averaging. Nevertheless, in this work, we decided to use intrinsic phase average, as it is still the most commonly used operator. This choice does not affect the issues and concepts studied here. The average phase pressure can be given by

$$P^{\alpha} = \frac{\sum_{j=1}^{n^{pb}} p_j^{\alpha} s_j^{\alpha} V_j}{\sum_{j=1}^{n^{pb}} s_j^{\alpha} V_j}, \ \alpha = n, w. \tag{17}$$

[43] The specific interfacial area was calculated by summing all the interfacial areas in an averaging domain divided by its total volume:

$$a^{nw} = \frac{\sum_{j=1}^{n^{pb}} A_j^{nw}}{V}, \tag{18}$$

where A_j^{nw} is the fluid-fluid interfacial area in a pore body j. The gradients of fluids pressures and specific interfacial area over the domain were also calculated using equations similar to (16). The average phase velocity for the domain centered at x was defined as follows:

$$\mathbf{v}^{\alpha} = \frac{\sum_{j=1}^{n^{pth}} \mathbf{v}_j^{\alpha} s_j^{\alpha} V_j}{\sum_{j=1}^{n^{pth}} s_j^{\alpha} V_j}, \ \alpha = n, w, \tag{19}$$

where $\mathbf{v}_j^{\alpha}$ is the local velocity in the pore throat j for fluid α and V_j is the volume of the pore throat j. This velocity is averaged over the pore throats considering their orientations.

[44] The macroscopic velocity of fluid-fluid interfaces can be determined in two different ways.

[45] 1. It can be based on the average of velocities of individual interfaces: It is indeed possible to calculate the velocity of individual interfaces within the network. However, this velocity fluctuates strongly. The reason is that interfaces move in the form of Haines jump. As long as the local capillary pressure is smaller than the entry capillary pressure of a pore throat, the pore interface is stagnant. But, once the interface moves, it moves very fast. At any given time, only a few interfaces can move, which temporarily may have large velocities. These velocities depend on the global capillary pressure, interfacial tension, pore size, and viscosity ratio. *Lu et al.* [1995] found that for ethanol-air system with a viscosity of 0.0119 Pa s, in a pore with radius of 0.05 cm, the velocity of capillary rise can reach 20 cm s^{-1}. So, these velocities are not really representative of all fluid-fluid interfaces in the averaging domain.

[46] 2. It can be based on the time rate of change of the centroids of all interfacial areas within the averaging domain: We propose that the second option is physically more acceptable and in line with the classical definition of the average velocity of a collection of masses since it is equal to the time rate of change of their center of mass. Therefore, we have chosen to determine the macroscale velocity of interfaces from the position of center of mass of interfaces in the averaging domain in two consecutive time steps. Given the assumption that fluid-fluid interfaces have a constant mass density, the macroscopic interfacial velocity was defined as follows:

$$\mathbf{w}^{nw} = \frac{1}{t^{k+1} - t^k} \left[\left(\frac{\sum_{j=1}^{n^{pb}} \mathrm{x}_j A_j^{nw}}{\sum_{j=1}^{n^{pb}} A_j^{nw}} \right)^{k+1} - \left(\frac{\sum_{j=1}^{n^{pb}} \mathrm{x}_j A_j^{nw}}{\sum_{j=1}^{n^{pb}} A_j^{nw}} \right)^{k} \right], \tag{20}$$

where x_j denoted the position of interfaces in pore body j and the superscript k denotes the time step. Note that in this calculation, only the interfaces in the pore bodies were included. Interfaces in pore throats did not move from one time step to another.

[47] For calculating the divergence of product of interfacial area and its velocity, $\nabla(a_i^{nw}\mathbf{w}_i^{nw})$, appearing in equation (4), we employ the 1-D equivalent of the divergence theorem:

$$\frac{\partial(a^{nw}\mathbf{w}^{nw})}{\partial x} = \frac{1}{\delta} \left[\sum_{j=1}^{n^{pb}} (A_j^{nw}\mathbf{w}_j^{nw})|_{\mathrm{DB}} - \sum_{j=1}^{n^{pb}} (A_j^{nw}\mathbf{w}_j^{nw})|_{\mathrm{UB}} \right], \tag{21}$$

where DB and UB denote the downstream and upstream boundaries, respectively.

4. Results and Discussion

[48] The extended two-phase flow equations involve new variables such as velocity of fluid-fluid interfaces or their rate of production, as well as new coefficients. In this section, the behavior of these new variables is investigated, and values of new coefficients are quantified. The major interest in this work is to gain an insight into the role of fluid-fluid interfaces in the description of two-phase flow.

4.1. Investigation of Darcy's Law

4.1.1. Equilibrium Conditions

[49] As explained in section 3, capillary pressure–saturation (P^c-S^w) curves were determined under quasi-static conditions, and phase permeability-saturation (k^{α}-S^w) curves were obtained through steady state flow simulations of primary drainage. These curves were computed for each and every moving averaging domain along our network. As a result of this procedure, 180 average curves were produced. The mean of resulting curves are shown in Figure 4, where the range of variations is shown by vertical bars. It is obvious that there is no significant variation in these characteristic curves over the whole network.

[50] Under no-flow conditions, we have $\mathbf{v}^{\alpha} = 0$ and $\partial P^{\alpha}/\partial x = 0$, but we may still have gradients in saturation and specific interfacial area. Thus, from equation (1), as there is no gravity in our simulations, we obtain

$$\frac{\Psi^{\alpha S}}{\Psi^{\alpha a}} = -\frac{a^{nw}_{,x}}{S^{w}_{,x}} \quad \alpha = w, n, \tag{22}$$

where $S_{,x}$ and $a_{,x}$ denote $\partial S/\partial x$ and $\partial a/\partial x$, respectively. From our simulation results, we can calculate the right-hand side of equation (22) at different saturation values as plotted in Figure 5. Note that $\Psi^{nS}/\Psi^{na} = \Psi^{wS}/\Psi^{wa}$. There is an obvious trend that can be fitted with a simple formula

$$\frac{\Psi^{wS}}{\Psi^{wa}} = \frac{m}{S^{wn}}, \tag{23}$$

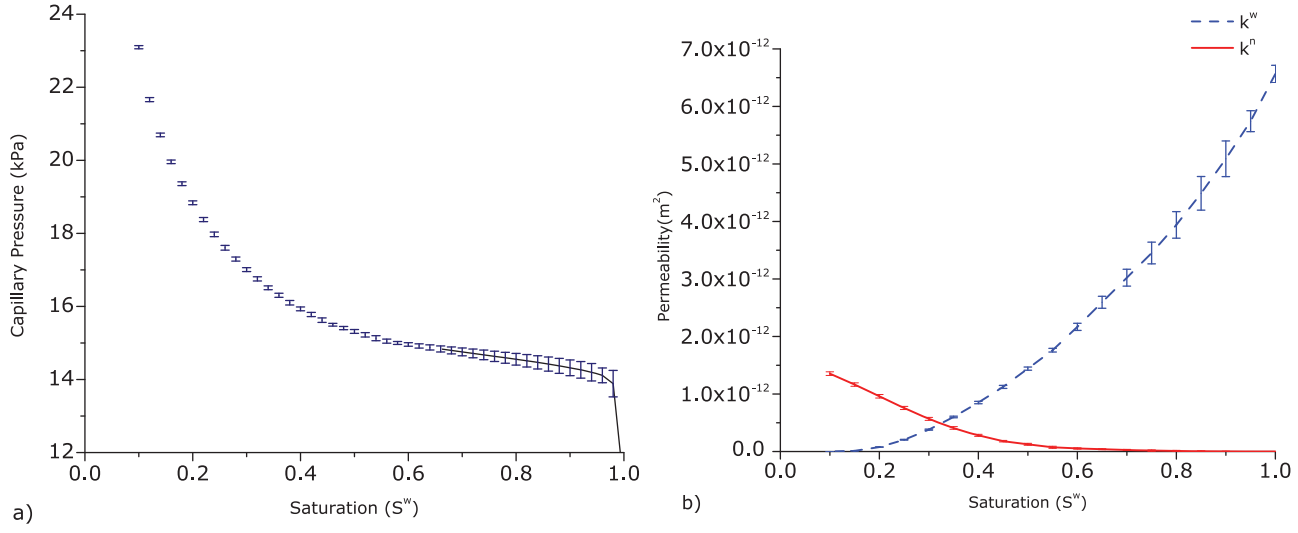

Figure 4. Averaged characteristic curves for a moving averaging domains along the domain. The bars at each saturation show the minimum and maximum value resulted at that saturation. (a) Capillary pressure–saturation curve. (b) Permeability for each fluid versus saturation.

where m has the dimension of $[1/L]$ and n is a dimensionless coefficient. For the curve presented in Figure 5, we have $m = 19.9\ \mathrm{mm}^{-1}$ and $n = 0.574$.

4.1.2. Standard Darcy's Law Under Transient Conditions

[51] The relative permeability curve, measured under steady state flow conditions, is also used in the standard Darcy's law under transient flow conditions. Here, we show that this assumption is generally not valid. In our transient simulations, we determined the phase permeability K^{α} by calculating $-\mu^{\alpha}\mathbf{v}^{\alpha}/\partial P^{\alpha}/\partial x$ for many averaging domains along the network (the same procedure that we followed to obtain curves shown in Figure 4). The mean of the resulting curves are plotted in Figure 6, along with the steady state curves.

[52] Our results clearly show that the steady state and transient curves are significantly different, specially for the nonwetting phase. There are large discrepancies between the steady state and transient permeability curves. In particular, it has a nonmonotonic behavior and is much larger than the steady state values for the medium and high wetting phase saturations. This is also the range that fluid-fluid interfaces are generated and the system is very dynamic. As known, the premise of the standard theory using Darcy's law is that the relative permeability determined under steady state flow conditions is also applicable under transient conditions. We have examined this matter and have clearly shown that this assumption is not supported by our numerical simulations as well as previous laboratorial studies [e.g., *Tsakiroglou et al.*, 2003]. When the system gets closer to the steady state conditions, the discrepancy between the curves decreases.

[53] As mentioned above, the permeability values are determined for a large number of averaging domains. The variations from the mean values are shown by means of vertical bars for the steady state curve and by vertical boxes for

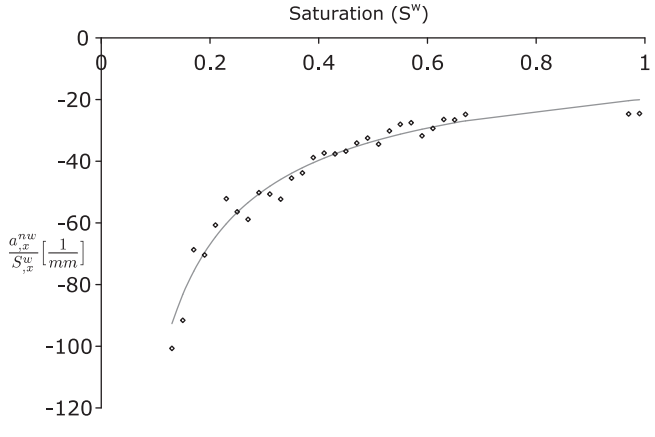

Figure 5. Variation of $a^{nw}_{,x}/S^{nw}_{,x}$ versus saturation for all snapshots using equations (15), (16), and (18). This ratio is used for quantifying the ratio of material coefficients $\Psi^{\alpha S}/\Psi^{\alpha a}$ in the extended Darcy's law (equation (1)).

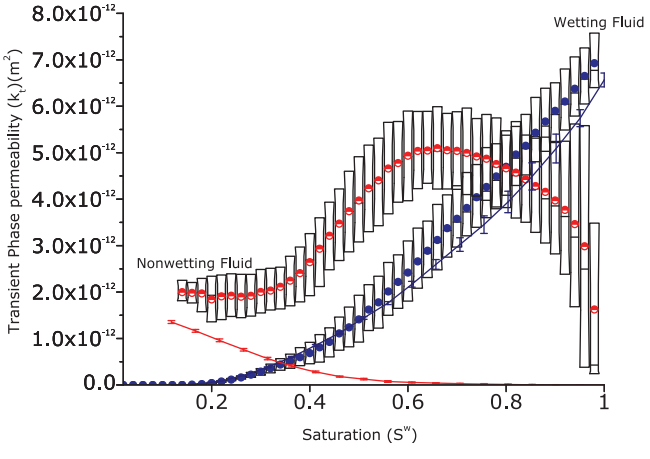

Figure 6. Ratio of α phase flux to the α phase pressure gradient under transient conditions, referred to as transient phase permeability (shown in circles). It is compared with steady state permeability curves (shown in solid lines). The bars show the range of variation of 10%–90% of the data points at the given saturation.

the transient curves. The boxes in Figure 6 show the 10% and 90% probability of the occurrence for all transient phase permeabilities. As it can be seen, there is a significant variation in the magnitude of the transient phase permeability. As mentioned before, in our simulations, capillary number was variable; it decreased with invasion of the nonwetting fluid.

[54] Also, it can be observed that under transient flow conditions, for $S^w > 0.5$, there is a linear relationship between the transient wetting phase permeability and saturation. This is qualitatively in agreement with steady state experimental observations of *Constantinides and Payatakes* [1996] and simulation results of *Tsakiroglou et al.* [2003], who observed that with the increase of capillary number (increase of viscous forces), the nonlinear behavior of relative permeability decreased.

[55] Furthermore, we note that as the residual saturation is approached, the transient nonwetting phase permeability also approaches the steady state values. This is because the fluids configuration is well developed under those conditions and nonequilibrium effects become negligible. The foregoing results point to the fact that the standard Darcy's law is not valid under transient flow conditions. We therefore investigate the role of additional terms in the extended Darcy's law given by equation (1).

4.1.3. Extended Darcy's Law Under Transient Conditions

[56] As mentioned before, many computational and experimental studies have shown that the relative permeability in the classical Darcy's law strongly depends on the transient flow variables such as flow velocity and/or pressure gradient. On the basis of the theoretical background [e.g., *Hassanizadeh and Gray*, 1993a] as well as our computational experiments, we propose that this is because the pressure gradient is not the only driving force for two-phase flow. Indeed, as suggested by equation (1), gradients in saturation and specific interfacial area also contribute to the flow. But, because they are absent in the classical Darcy's law, their role has to be taken over by the relative permeability. In order to investigate this conjecture, we use the results of transient conditions to determine the significance of extra terms in equation (1). First, the values of coefficients $\Psi^{\alpha S}$ and $\Psi^{\alpha a}$ need to be determined.

[57] In section 4.1.2, the ratio of $\Psi^{\alpha S}/\Psi^{\alpha a}$ for each phase was obtained; thus, only two independent coefficients (one coefficient per phase) should be determined. Once again, for any given set of boundary conditions, $\mathbf{v}^\alpha$, $P^\alpha_{,x}$, $a^{nw}_{,x}$, and $S^w_{,x}$ can be calculated. With K^α already known as a function of S^w for steady state simulations, the other two coefficients can be calculated. The results are shown Figure 7. One should note that the data points correspond to various dynamic conditions (flow rates) along the domain. Yet the material coefficients, $\Psi^{\alpha a}$ and $\Psi^{\alpha S}$, seem to be independent of dynamic conditions, and there is a clear trend as a function of saturation. The large variations in the values of these material coefficients near $S^w = 1$ are due to the fact that at that saturation, the two-phase flow occurs in a small number of pores and the addition or subtraction of one pore may have a large effect on average variables. As a result, the values of these coefficients at high saturation are uncertain.

[58] To show the importance of the gradient of pressure compared to the new terms in the extended Darcy's law, we have presented their ratio in Figure 8. In Figure 8a the ratio $P^w_{,x}\Big/\left(-\Psi^{wa}a^{nw}_{,x} - \Psi^{wS}S^w_{,x}\right)$ versus saturation and in Figure 8b the ratio $\left(-\Psi^{na}a^{nw}_{,x} + \Psi^{nS}S^w_{,x}\right)\Big/P^n_{,x}$ versus saturation have been presented. It is clear that the effect of the new terms is basically negligible for the wetting phase but very significant for the nonwetting phase. This means that the deviation of the fluid flux calculated from the classical Darcy's law from the "true value" is not as significant for the wetting phase as for the nonwetting fluid flux. In Figure 8b, the ratio $\left(-\Psi^{na}a^{nw}_{,x} + \Psi^{nS}S^w_{,x}\right)\Big/P^n_{,x}$ starts from a large value at high saturations, and it decreases as steady state conditions are approached. This implies that for an improved estimation of fluid fluxes under transient conditions, especially for the nonwetting fluid, the gradient of interfacial area and saturation should be included.

4.2. Interfacial Area Equations

[59] The introduction of the specific interfacial area as a state variable into the theories of multiphase flow necessitates a new set of governing equations to model its evolution. These are given by equations (2) and (4). Equations (2) and (4) also comprise new material properties, which are the macroscopic interface velocity, interfacial conductivity tensor, macroscale interfacial tension, material coefficient Ψ^{nw}, and the interfacial production term E^{nw}. In this section, the results of transient drainage simulations are used to calculate these properties and investigate their behavior.

4.2.1. Macroscopic Interface Velocity

[60] Using equation (20), the macroscopic interface velocity was calculated for 180 averaging domains with time. We then looked into the possible relationships between the interface velocity and other quantities. We found a meaningful relationship with the saturation and time rate of change of saturation. The resulting plot is shown in Figure 9a. As it can be observed, there is an almost linear relationship between the interface velocity and the time rate of saturation change. We should point out the small negative interface velocities were obtained at large saturations. This is caused by the fact that when interfaces have just entered the averaging domain, local imbibition may occur; that is, the nonwetting fluid may temporarily move back and out of the domain. In the intermediate saturation range, the interface velocity reaches its maximum value. *Nordhaug et al.* [2003] also calculated variation of interface velocity with saturation, using a pore network model with circular cross sections and a size of $10 \times 10 \times 50$ pore bodies, elongated in flow direction. They studied the variation of interface velocity under various transient conditions (capillary number and viscosity ratio). Although the algorithm for calculation of interface velocity in their network was different from our approach, they got a qualitatively similar behavior for interface velocity especially under capillary-dominated flow conditions. However, because of the small size of their averaging domain ($10 \times 10 \times 10$ pores), there was a boundary effect in their results, which caused an overshoot of interface velocity at large saturations ($S^w > 0.9$).

[61] We should emphasize that we are not seeking an explicit relationship between macroscopic interface velocity and saturation and its rate of change. Figure 9a is provided

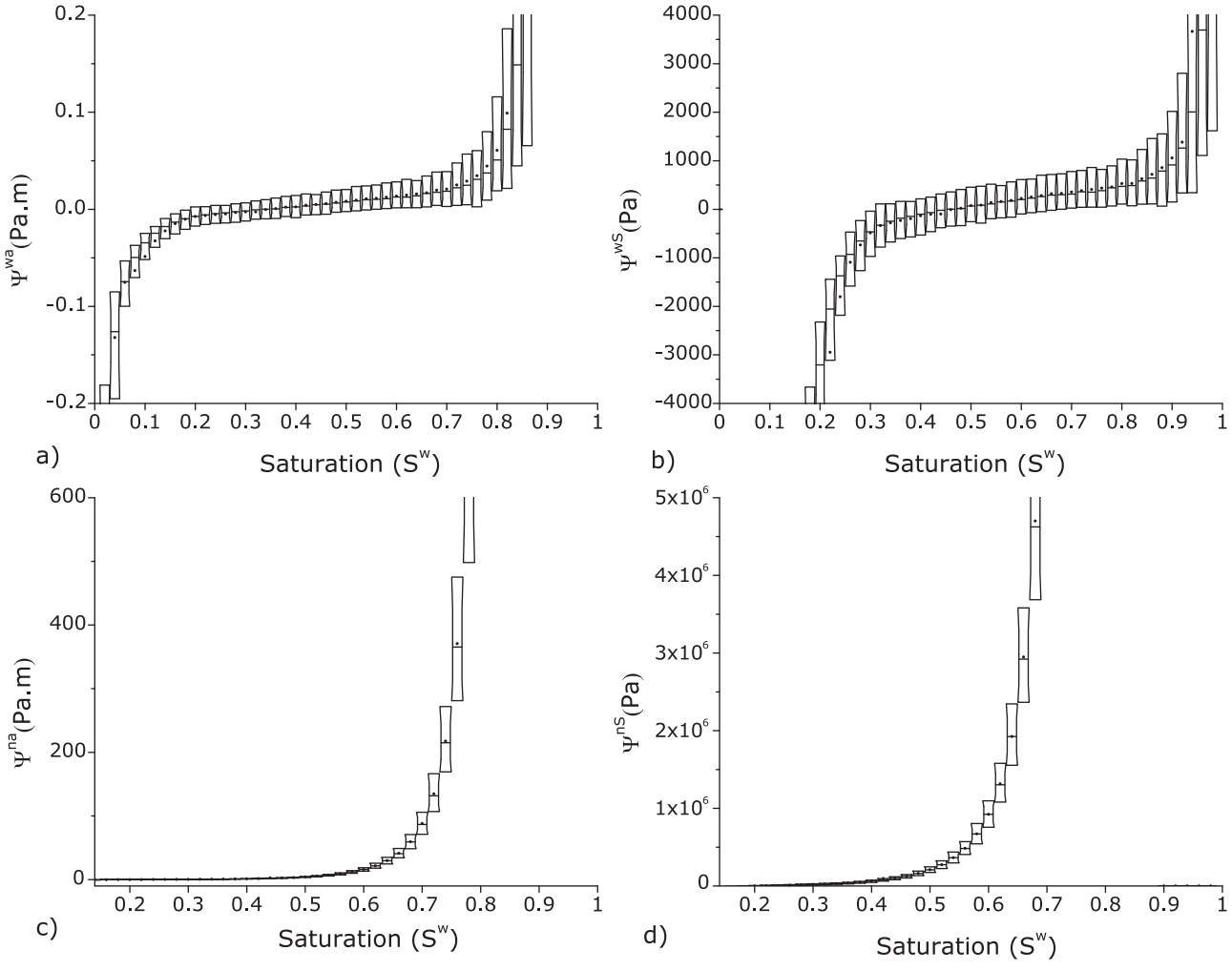

Figure 7. Variation of material properties presented in equation (1) based on the moving averaging domain analysis of the simulations. (a) Ψ^{wa}, (b) Ψ^{wS}, (c) Ψ^{na}, and (d) Ψ^{nS}. Description of the bars are given in caption of Figure 6.

here for the purpose of illustrating variations in interface velocity. The governing equation for describing the macroscopic motion of interfaces is equation (2) that will be investigated below.

4.2.2. Interface Conductivity and Material Coefficient Ψ^{nw}

[62] After calculating the fluid-fluid interface velocities at different saturations under variable transient conditions, it is possible to estimate the conductivity of interfaces using equation (2). Assuming constant interfacial compositions and for a one-dimensional domain, we can rewrite equation (2) as follows:

$$\mathbf{w}^{nw} = -k^{nw}(a^{nw}_{,x} + \psi^{nw} S^{w}_{,x}), \tag{24}$$

where $k^{nw}[L^3/T] = \sigma^{nw}\mathsf{K}^{nw}$ interfacial tension σ^{nw} is lumped into other coefficients, and $\psi^{nw} = \Psi^{nw}/\sigma^{nw}[1/L]$. First, the coefficient ψ^{nw} is obtained from the equilibrium conditions, where the interfaces do not move and $\mathbf{w}^{nw}$ is equal to zero. Under these conditions, we have

$$\psi^{nw} = -\frac{a^{nw}_{,x}}{S^{w}_{,x}} = \frac{m}{S^{wn}}, \tag{25}$$

where the right-hand side of equation (25) follows from equation (23). Next, the interfacial conductivity k^{nw} can be determined from equation (2) under transient conditions. All terms in equation (2) can be calculated for a large number of averaging domains and at various times, allowing us to find values of k^{nw} for a wide range of transient conditions. The result is plotted as a function of average saturation in Figure 9b. It is evident that the interface conductivity is an increasing function of wetting fluid saturation. One should note that, except for the range of $S^w > 0.9$, the variation in values of interface conductivity estimated under various transient conditions is not significant. This shows that this coefficient is a reasonably well-behaved function of saturation under a wide range of transient conditions. Large variations of interface conductivity for $S^w > 0.9$ is due to the variations of interface velocity. Negative values in that range (see Figure 9a) are caused by local temporary imbibition during the early stages of invasion. This effect reduces dramatically as soon as the nonwetting phase saturation becomes significant in the averaging domain.

4.2.3. Production Rate of Interfacial Areas

[63] We use equation (4) to calculate the production term, E^{nw}. Thus, we have to estimate the change of specific

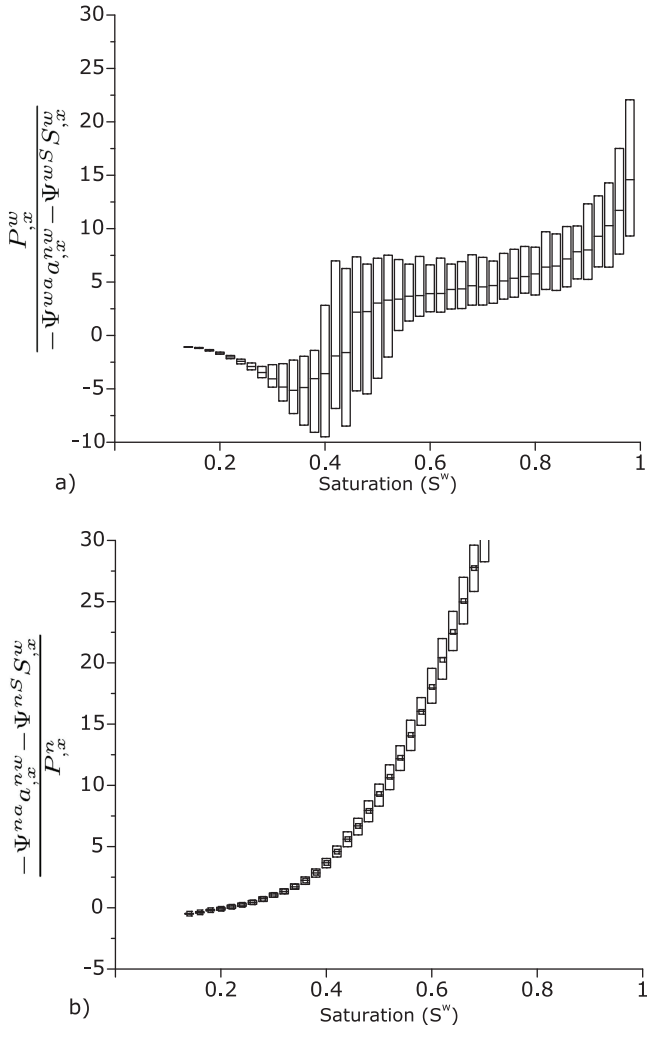

Figure 8. Ratio of gradient of fluid pressure to the other added terms in equation (1) for (a) wetting fluid (b) nonwetting fluid. On should note that for clear illustration the ratio is inverse in Figure 8b.

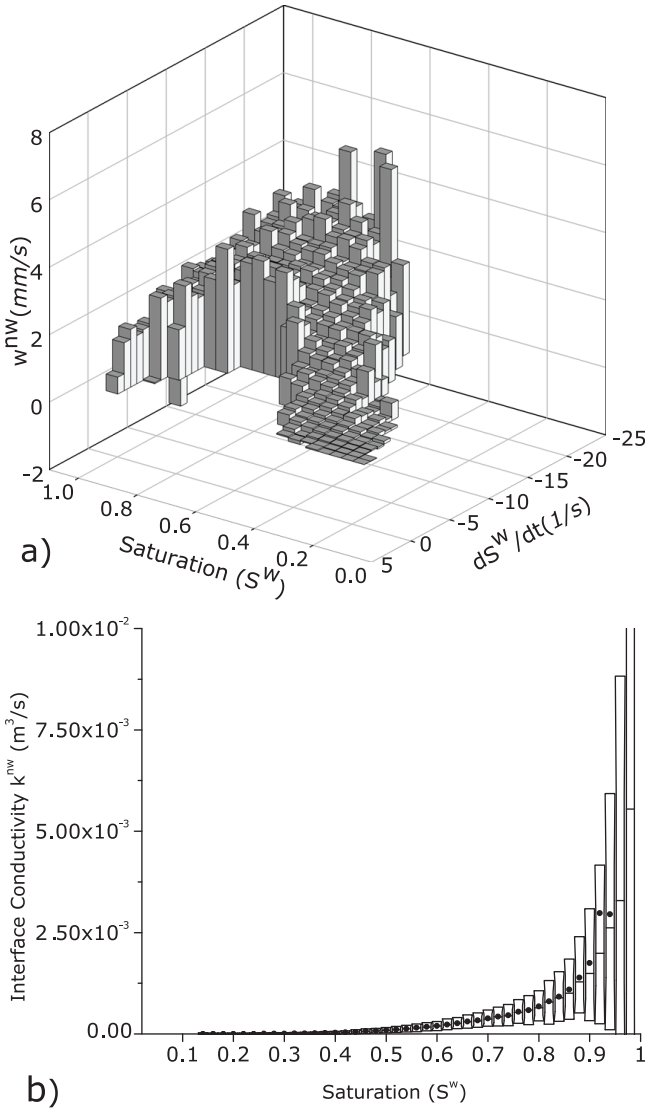

Figure 9. (a) Dependence of macroscopic interface velocity on saturation and change of saturation with time, calculated using equation (20) for all simulation snapshots and averaging domains, (b) Variation of interface conductivity with saturation resulted from analysis of all moving averaging domains in time and space. Description of the bars is given in the caption of Figure 6.

interfacial area with time $(\partial a^{nw}/\partial t)$ as well as the flux of interfacial area $(\partial(a^{nw}\mathbf{w}^{nw})/\partial x)$. Both of these quantities can be calculated for a large number of averaging domains. The resulting production rate is plotted in Figure 10 as a function of average saturation and its time rate of change. Figure 10 shows that E^{nw} depends linearly on the time rate of saturation change. Furthermore, it reaches its maximum value in the range of intermediate saturations. This is due to the greater possibilities for the creation of invasion sites at intermediate saturations. At high wetting fluid saturations, only a few pores are filled with the nonwetting fluid. Thus, a small amount of interfacial area is created. With invasion of the nonwetting fluid, more pores will be filled, each of them acting as the launching site for the invasion of many other pores by the nonwetting fluid. This causes a faster creation of interfacial area. Eventually, the interfacial area associated with the main terminal interfaces will start to become less and less, as many of them will coalesce with each other. Thus, the production rate of specific interfacial area will decrease.

5. Concluding Remarks

[64] We have simulated two-phase drainage experiments using a dynamic pore network model, called DYPOSIT, under constant pressure boundary conditions. The simulation network has a cross section of 30 × 30 pore bodies and a length of 210 pore bodies in the flow direction. The analyses are based on the volumetric averaging in a moving averaging domain with the size of 30 × 30 × 30 pore bodies. The averaging is done along the domain in many time steps. Because of the imposed boundary conditions (i.e., constant pressures) the flow velocity varies considerably with time as the nonwetting fluid invades the domain. As a result, the capillary number changes through the network with time from 2×10^{-5} to 5×10^{-7}. So, the

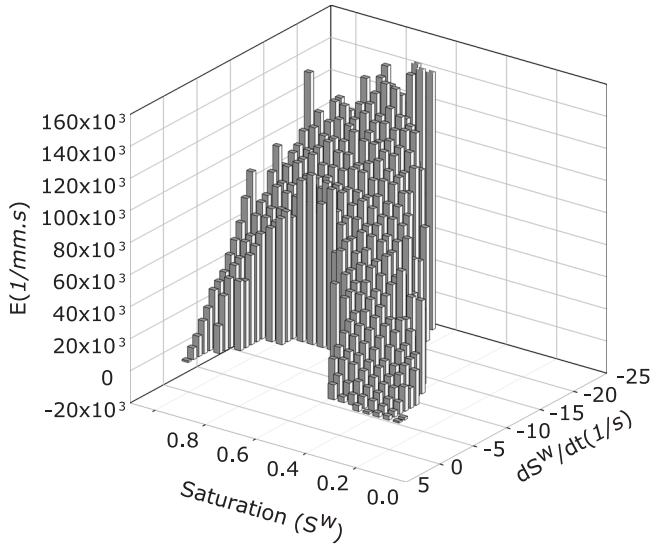

Figure 10. Dependence of production rate of specific interfacial area versus saturation and change of saturation with time based on equation (4) and calculated using equations (18) and (21) for all simulation snapshots and averaging domains.

calculated material properties are obtained for a wide range of capillary numbers.

[65] We have used our results to investigate the thermodynamically based theories of two-phase flow in porous media, where the fluid-fluid specific interfacial area is included as a new state variable. First, we have shown that if the standard Darcy's law is used under transient conditions, then the phase conductivity of the nonwetting phase will be a nonmonotonic function of saturation. Also, the wetting phase conductivity determined under transient conditions will be significantly different from the steady state phase conductivity. We propose that this is because of the fact that in the standard Darcy's law, the pressure gradient is assumed to be the only driving force for the flow. But, we know that in two-phase flow, the movement of interfaces and energies associated with them significantly affect the flow of phases. It is conjectured that the new terms in the extended Darcy equation account for such effects. These terms introduce gradients in the saturation and specific interfacial area as extra driving forces. We have shown that including these terms allows us to use the steady state relative permeability curve for transient flow conditions. We have determined the values of material coefficients associated with the extra terms that are well-behaved functions of saturation. Next, various coefficients appearing in the equations governing the evolution of interfaces were determined. One of these coefficients was the interface conductivity. Our results show that the interface conductivity is an increasing function of the wetting phase saturation. We have also determined the rate of production of specific interfacial area. Our results show a linear relationship between the production rate of fluid-fluid interfaces and the change of saturation with time. It is also shown that although interfaces may have high velocities at the moment of Haines jump, the macroscopic interface velocities are strongly correlated with the time rate of saturation change. Variation of macroscopic interfacial velocity with saturation, in an averaging domain, is nonmonotonic, having a maximum in the intermediate saturations.

[66] These analyses lead us to a new understanding that including gradient of interfacial area and the gradient of saturation in the new equations can implicitly account for the moving boundary between the two fluids during drainage. This feature is absent in the classical equations for two-phase flow. Dependence of the new parameters on fluid and porous medium properties is an important issue, which should be investigated in future. It must be noted that here we did not investigate the nonequilibrium capillarity effect (the second term in the right-hand side of equation (7)) as this was done extensively in the earlier work by *Joekar-Niasar et al.* [2010a] and *Joekar-Niasar and Hassanizadeh* [2010].

References

Aker, E., K. J. Maloy, A. Hansen, and G. G. Batrouni (1998), A two-dimensional network simulator for two-phase flow in porous media, *Transp. Porous Media*, *32*, 163–186.

Al-Gharbi, M. S., and M. J. Blunt (2005), Dynamic network modeling of two-phase drainage in porous media, *Phys. Rev. E*, *71*, 016308, doi:10.1103/PhysRevE.71.016308.

Buyevich, Y. A. (1995), Towards a theory of nonequilibrium multiphase filtration flow, *Transp. Porous Media*, *21*, 145–162.

Cheng, J.-T., L. J. Pyrak-Nolte, D. D. Nolte, and N. J. Giordano (2004), Linking pressure and saturation through interfacial area in porous media, *Geophys. Res. Lett.*, *31*, L08502, doi:10.1029/2003GL019282.

Constantinides, G. N., and A. C. Payatakes (1996), Network simulation of steady-state two-phase flow in consolidated porous media, *AIChE J.*, *42*, 369–382.

Dahle, H. K., and M. A. Celia (1999), A dynamic network model for two-phase immiscible flow, *Comput. Geosci.*, *3*, 1–22.

Dias, M. M., and A. C. Payatakes (1986a), Network models for two-phase flow in porous media Part 1. immiscible microdisplacement of nonwetting fluids, *J. Fluid Mech.*, *164*, 305–336.

Dias, M. M., and A. C. Payatakes (1986b), Network models for two-phase flow in porous media Part 2. motion of oil ganglia, *J. Fluid Mech.*, *164*, 337–358.

Entov, V. M. (1980), Theory of nonequilibrium effects associated with the flow of nonuniform fluids in porous media, *Fluid Dyn.*, *15*(3), 365–369, doi:10.1007/BF01089969.

Ferer, M., W. N. Sams, R. A. Geisbrecht, and D. H. Smith (1993), Crossover from fractal to compact flow from simulations of two-phase flow with finite viscosity ratio in two dimensional porous media, *Phys. Rev. E*, *47*(4), 2713–2723.

Fernández, J. F., R. Rangel, and J. Rivero (1991), Crossover length from invasion percolation to diffusion-limited aggregation in porous media, *Phys. Rev. Lett.*, *67*(21), 2958–2961.

Gielen, T., S. M. Hassanizadeh, A. Leijnse, and H. F. Nordhaug (2005), Dynamic effects in multiphase flow: A pore-scale network approach, in *Upscaling Multiphase Flow in Porous Media*, edited by D. B. Das and S. M. Hassanizadeh, pp. 217–236, Springer, New York.

Goode, P. A., and T. S. Ramakrishnan (1993), Momentum transfer across fluid-fluid interfaces in porous media: A network model, *AIChE J.*, *39* (7), 1124–1134.

Hassanizadeh, S. M., and W. G. Gray (1990), Mechanics and thermodynamics of multiphase flow in porous media including interphase boundaries, *Adv. Water Resour.*, *13*, 169–186.

Hassanizadeh, S. M., and W. G. Gray (1993a), Thermodynamic basis of capillary pressure in porous media, *Water Resour. Res.*, *29*, 3389–3405, doi:10.1029/93WR01495.

Hassanizadeh, S. M., and W. G. Gray (1993b), Toward an improved description of the physics of two-phase flow, *Adv. Water Resour.*, *16*, 53–67.

Hassanizadeh, S. M., M. A. Celia, and H. K. Dahle (2002), Dynamic effects in the capillary pressure–saturation relationship and their impacts on unsaturated flow, *Vadose Zone J.*, *1*, 38–57, doi:10.2113/1.1.38

Hughes, R. G., and M. J. Blunt (2000), Pore scale modeling of rate effects in imbibition, *Transp. Porous Media*, *40*, 295–322.

Joekar-Niasar, V., and S. M. Hassanizadeh (2011), Analysis of fundamentals of two-phase flow in porous media using dynamic pore-network models: A review, *Crit. Rev. Environ. Sci. Technol.*, in press.

Joekar-Niasar, V., and S. M. Hassanizadeh (2010), Effect of fluids properties on non-equilibrium capillarity effects: Dynamic pore-network modeling, *Int. J. Multiphase Flow*, *37*, 198–214, doi:10.1016/j.ijmultiphaseflow.2010.09.007.

Joekar-Niasar, V., S. M. Hassanizadeh, and A. Leijnse (2008), Insights into the relationships among capillary pressure, saturation, interfacial area and relative permeability using pore-network modeling, *Transp. Porous Media*, *74*(2), 201–219, doi:10.1007/s11242-007-9191-7.

Joekar-Niasar, V., S. M. Hassanizadeh, L. J. Pyrak-Nolte, and C. Berentsen (2009), Simulating drainage and imbibition experiments in a high-porosity micromodel using an unstructured pore network model, *Water Resour. Res.*, *45*, W02430, doi:10.1029/2007WR006641.

Joekar-Niasar, V., S. M. Hassanizadeh, and H. K. Dahle (2010a), Non-equilibrium effects in capillarity and interfacial area in two-phase flow: Dynamic pore-network modelling, *J. Fluid. Mech.*, *655*, 38–71, doi:10.1017/S0022112010000704.

Joekar-Niasar, V., M. Prodanović, D. Wildenschild, and S. M. Hassanizadeh (2010b), Network model investigation of interfacial area, capillary pressure and saturation relationships in granular porous media, *Water Resour. Res.*, *46*, W06526, doi:10.1029/2009WR008585.

Kalaydjian, F., and C. M. Marle (1987), Thermodynamic aspects of multiphase flow in porous media, *Collect. Colloq. Semin. Inst. Fr. Pet.*, *45*, 513–531.

Koplik, J., and T. J. Lasseter (1985), Two-phase flow in random network models of porous media, *Soc. Pet. Eng. J.*, *25*, 89–110, doi:10.2118/11014-PA.

Korteland, S., S. Bottero, S. M. Hassanizadeh, and C. W. J. Berentsen (2009), What is the correct definition of macroscale pressure?, *Transp. Porous Media*, *84*, 153–175, doi:10.1007/s11242-009-9490-2.

Koval, E. J. (1963), A method for predicting the performance of unstable miscible displacement in heterogenous media, *Soc. Pet. Eng. J.*, *3*(2), 145–154.

Li, L., C. A. Peters, and M. A. Celia (2007), Reply to "Comment on upscaling geochemical reaction rates using pore-scale network modeling" by Peter C. Lichtner and Qinjun Kang, *Adv. Water Resour.*, *30*(3), 691–695, doi:10.1016/j.advwatres.2006.05.002.

Lu, T. X., J. W. Biggar, and D. R. Nielsen (1994), Water movement in glass bead porous media: 1. Experiments of capillary rise and hysteresis, *Water Resour. Res.*, *30*(12), 3275–3281, doi:10.1029/94WR00997.

Lu, T. X., D. R. Nielsen, and J. W. Biggar (1995), Water movement in glass bead porous media: 3. Theoretical analysis of capillary rise into initially dry media, *Water Resour. Res.*, *31*(1), 11–18, doi:10.1029/94WR00999.

Mason, G., and N. R. Morrow (1987), Meniscus configurations and curvatures in non-axisymmetric pores of open and closed uniform cross section, *Proc. R. Soc. London, Ser. A*, *414*(1846), 111–133.

Mogensen, K., and E. H. Stenby (1998), A dynamic two-phase pore-scale model for imbibition, *Transp. Porous Media*, *32*, 299–327.

Niessner, J., and S. M. Hassanizadeh (2008), A model for two-phase flow in porous media including fluid-fluid interfacial area, *Water Resour. Res.*, *44*, W08439, doi:10.1029/2007WR006721.

Niessner, J., and S. M. Hassanizadeh (2009a), Modeling kinetic interphase mass transfer for two-phase flow in porous media including fluid-fluid interfacial area, *Transp. Porous Media*, *80*, 329–344, doi:10.1007/s11242-009-9358-5.

Niessner, J., and S. M. Hassanizadeh (2009b), Non-equilibrium interphase heat and mass transfer during two-phase flow in porous media-theoretical considerations and modeling, *Adv. Water Resour.*, *32*, 1756–1766, doi:10.1016/j.advwatres.2009.09.007.

Nordbotten, J. M., M. A. Celia, H. K. Dahle, and S. M. Hassanizadeh (2007), Interpretation of macroscale variables in Darcy's law, *Water Resour. Res.*, *43*, W08430, doi:10.1029/2006WR005018.

Nordbotten, J. M., M. A. Celia, H. K. Dahle, and S. M. Hassanizadeh (2008), On the definition of macroscale pressure for multiphase flow in porous media, *Water Resour. Res.*, *44*, W06S02, doi:10.1029/2006WR005715.

Nordhaug, H. F., M. Celia, and H. K. Dahle (2003), A pore network model for calculation of interfacial velocities, *Adv. Water Resour.*, *26*, 1061–1074, doi:10.1016/S0309-1708(03)00100-3.

Pereira, G. G., W. V. Pinczewski, D. Y. C. Chan, L. Paterson, and P. E. Øren (1996), Pore-scale network model for drainage-dominated three-phase flow in porous media, *Transp. Porous Media*, *24*, 167–201.

Pop, I. S., C. J. van Duijn, J. Niessner, and S. M. Hassanizadeh (2009), Horizontal redistribution of fluids in a porous medium: The role of interfacial area in modeling hysteresis, *Adv. Water Resour.*, *32*, 383–390, doi:10.1016/j.advwatres.2008.12.006.

Porter, M. L., M. G. Schaap, and D. Wildenschild (2009), Lattice-Boltzmann simulations of the capillary pressure-saturation-interfacial area relationship for porous media, *Adv. Water Resour.*, *32*, 1632–1640, doi:10.1016/j.advwatres.2009.08.009.

Prat, M. (2002), Recent advances in pore-scale models for drying of porous media, *Chem. Eng. J.*, *86*, 153–164, doi:10.1016/S1385-8947(01)00283-2.

Reeves, P. C., and M. A. Celia (1996), A functional relationship between capillary pressure, saturation, and interfacial area as revealed by a pore-scale network model, *Water Resour. Res.*, *32*, 2345–2358, doi:10.1029/96WR01105.

Sorbie, K. S., H. R. Zhang, and N. B. Tsibuklis (1995), Linear viscous fingering: New experimental results, direct simulation and the evaluation of averaged models, *Chem. Eng. Sci.*, *50*(4), 601–616, doi:10.1016/0009-2509(94)00252-M.

Stauffer, F. (1978), Time dependence of the relations between capillary pressure, water content and conductivity during drainage of porous media, paper presented at Symposum on Scale Effects in Porous Media, Int. Assoc. for Hydro-Environ. Eng., Thessaloniki, Greece, 29 Aug. to 1 Sept.

Tallakstad, K. T., G. Løvoll, H. A. Knudsen, T. Ramstad, E. G. Flekkøy, and K. J. Måløy (2009), Steady-state, simultaneous two-phase flow in porous media: An experimental study, *Phys. Rev. E*, *80*(3), 036308, doi:10.1103/PhysRevE.80.036308.

Theodoropoulou, M., V. Sygouni, V. Karoutsos, and C. D. Tsakiroglou (2005), Relative permeability and capillary pressure functions of porous media as related to the displacement growth pattern, *Int. J. Multiphase Flow*, *31*, 1155–1180, doi:10.1016/j.ijmultiphaseflow.2005.06.009.

Thompson, K. E. (2002), Pore-scale modeling of fluid transport in disordered fibrous materials, *AIChE J.*, *48*, 1369–1389, doi:10.1002/aic.690480703.

Tsakiroglou, C. D., M. A. Theodoropoulou, and V. Karoutsos (2003), Non-equilibrium capillary pressure and relative permeability curves of porous media, *AIChE J.*, *49*, 2472–2486, doi:10.1002/aic.690491004.

Washburn, E. W. (1921), The dynamics of capillary flow, *Phys. Rev.*, *17*(3), 273–283.

Whitaker, S. (1977), Simultaneous heat, mass, and momentum transfer in porous media: A theory of drying, *Adv. Heat Transfer*, *13*, 119–200.

Wilkinson, D. (1986), Percolation effects in immiscible displacement, *Phys. Rev. A*, *34*(2), 1380–1391.

Yang, D., R. P. Currier, and D. Z. Zhang (2009), Ensemble phase averaged equations for multiphase flows in porous media. Part 1: The bundle-of-tubes model, *Int. J. Multiphase Flow*, *35*, 628–639, doi:10.1016/j.ijmultiphaseflow.2009.03.002.

Zhang, D. Z., W. B. VanderHeyden, Q. Zou, and N. T. Padial-Collins (2007), Pressure calculations in disperse and continuous multiphase flows, *Int. J. Multiphase Flow*, *33*, 86–100, doi:10.1016/j.ijmultiphaseflow.2006.07.006.

S. M. Hassanizadeh and V. Joekar-Niasar, Environmental Hydrogeology Group, Department of Earth Sciences, Utrecht University, PO Box 80021, Utrecht, NL-3508 TA, Netherlands. (joekar@geo.uu.nl)